INAF/OATs, UNIMi
LFI Project System Team

Planck LFI

TITLE: **PLANCK/LFI: Flight Effects on the REBA Parameters Optimization**

DOC. TYPE: Technical Note
PROJECT REF.: PL-LFI-OAT-TN-063 PAGE: 1 of 30
ISSUE/REV.: 0.1 DATE: July 31, 2009

Prepared by	Michele Maris Maurizio Tomasi	July 31, 2009
Agreed by	M. Bersanelli LFI Instrument Scientist C.R. Butler LFI Program Manager	??? ???
Approved by	N. Mandolesi LFI Principal Investigator	???

CHANGE RECORD

Issue	Date	Sheet	Description of change	Release
0.0	06th July, 2009	All	First analysis	0.0
0.1	20th July, 2009	All	First draft started	0.1
0.2	31st July, 2009	All	First draft issue of document	0.2

DISTRIBUTION LIST

Recipient	Company/Institute	E-mail address	Sent
N. Mandolesi	INAF-IASF Bologna	reno@bo.iasf.cnr.it	Yes
C. Butler	INAF-IASF Bologna	butler@bo.iasf.cnr.it	Yes
M. Bersanelli	Univ. di Milano	marco.bersanelli@fisica.unimi.it	Yes
A. Mennella	Univ. di Milano	daniele.mennella@fisica.unimi.it	Yes
M. Tomasi	Univ. di Milano	maurizio.tomasi@unimi.it	Yes
M. Balasini	TAS-F Milano	balasini.m@thalesaleniaspace.com	Yes
R. Silvestri	TAS-F Milano	silvestri.r@thalesaleniaspace.com	Yes
P. Leutenegger	TAS-F Milano	leutenegger.p@thalesaleniaspace.com	Yes
M. Miccolis	TAS-F Milano	miccolis.m@thalesaleniaspace.com	Yes
G. Cafagna	TAS-F Milano	cafagna.g@thalesaleniaspace.com	Yes
F. Bertini	ESA	federico.bertini@esa.int	Yes
L. Perez Cuevas	ESA	leticia.perez.cuevas@esa.int	Yes
O. Piersanti	ESA	osvaldo.piersanti@esa.int	Yes
J.P. Chambelland	TAS-F Cannes	jean-philippe.chambelland@thalesaleniaspace.com	Yes
B. Collaudin	TAS-F Cannes	bernard.collaudin@space.alcatel.fr	Yes
P. Rihet	TAS-F Cannes	patrick.rihet@thalesaleniaspace.com	Yes
N. Seville	TAS-F Cannes	norbert.seville@thalesaleniaspace.com	Yes
J.P. Hayet	TAS-F Cannes	jean-pierre.hayet@thalesaleniaspace.com	Yes
A. Gregorio	Univ. di Trieste	anna.gregorio@ts.infn.it	Yes
M. Maris	INAF-OAT Trieste	maris@oats.inaf.it	Yes
A. Zacchei	INAF-OAT Trieste	zacchei@oats.inaf.it	Yes

Contents

LIST OF ABBREVIATIONS

acronym	**Explanation**
LFI	Low Frequency Instrument

1 Applicable and Reference Documents

Applicable Documents

[AD-1] Maris, M., Tomasi, M., Galeotta, S., et al.
Optimization of PLANCK/LFI onboard data handling
2009, LFI / Prelaunch Paper D2

[AD-2] Mennella, A., et al.
doc about r factor accuracy

Reference Documents

[RD-1] Tomasi, M., Maris, M.,
report calibrazione reba
PL-LFI-OAT-TN-???

[RD-2] Maris, M., Maino, D., Burigana, C., Mennella, A., Bersanelli, M., Pasian, F.
The effect of signal digitisation in CMB experiments
A&A, 2004, 777 - 794

[RD-3] Maris, M., Maino, D., Burigana, C., Mennella, A., Bersanelli, M., Pasian, F.
The effect of signal digitisation in CMB experiments
A&A, 2004, 777 - 794

2 Scope of the document

This document reports an analysis of the differences among the REBA parameters optimazion in CSL and in Flight.

Such differences arise from

1. presence of a sky signal, in particular the cosmological dipole;
2. different operative conditions;
3. 4K cooler fluctuations;
4. additive constraints to the maximum acceptable processing error which where not considered in CSL.

Among the possible additive constrains the most important are:

1. to limit the processing error in total power;
2. to limit the impact of onboard processing on the r deterermination.

All of these effects asks to improve the OCA2 optimization procedures in order to have a program adapted to flight conditions.

This does not require large modification of OCA2, in most cases it is a matter to add more tests at the output of the application or to use OCA2 in a different manner.

However, this could have an impact on the overall speed of the optimization procedure.

In the following we will denote with OCA2@CSL the version of OCA2 operated at CSL, and with OCA2@FLIGHT the OCA2 optimizzation algorithm updated for Flight.

2.1 Limits of Applicability

This note have been started before the first run of the REBA calibration procedure.

Consequently part of the analysis are based on CSL data or early flight data.

This report is just illustrative of the effects and does not represent a complete quantitative assessement.

The report assumes thet reader already knows the procedure and problems of LFI REBA compression and calibration.

3 A brief introduction at OCA2@CSL

OCA2@CSL is the code used to optimize the REBA parameter during the CSL, and it is able to optimize the parameters by using two methods:

1. numerical optimization based on the same code used for omboard processing and compression (a module called `OCA2K` which represents a complete *onboard processing emulator*);
2. analytical optimization based on an approximation of the real data.

The need for the analytical approximation comse from thet fact that the numerical optimization is very slow. Too slow for the time constraints for the REBA optimization in CSL and during the CPV phase.

3.1 The analytical model

The analytical approximation in OCA2@CSL is based on the following hypothesis on the AVR1 signal feeded by the SPU at the compressor:

1. AVR1 are interlaced sequences of sky and ref signals;
2. both sky and ref signals are realizzations of stationary random noises with not null expectations, nornal distributed, possibly correlated
3. $1/f$ noise is not relevant at the scale of a packet;
4. expectations for sky and ref could be different;
5. sky and ref does not contain any deterministic component (either periodical, or aperiodical)

examples of deterministic signals are drifts, 4K ref fluctuations, the cosmological dipole.

It is evident from this premise that it can not be taken for grant that OCA2@CSL will be completely able to perform the REBA optimization in flight without some additional validation test on real data.

3.2 Optimization algorithm

It is important to remember how OCA2@CSL optimizes the REBA parameters.

1. OCA2@CSL gets a chunck of AVR1 data from the REBA for a given detector, a list of r_1, r_2 parameters to be testsed and an optimal compression rate $C_{\mathrm{r}}^{\mathrm{opt}}$;
2. at first OCA2@CSL uses an analytical model, based on the assumptions above, to optimize the r_1, r_2 parameters (defined over a grid with a given, finite resolution) and estimate the q_{opt}, to do this
   (a) OCA2@CSL uses an analytical model for the function of merith $\Gamma_X(r_1, r_2)$, and find the r_1, r_2 which maximizes $\gamma(r_1, r_2)$;
   (b) for the optimized (r_1, r_2) OCA2@CSL uses `OCA2K` to map the real C_{r} as a function of q_{opt}, for the given (r_1, r_2);
   (c) by polynomial interpolation determines the q_{opt} corresponding at $C_{\mathrm{r}} = C_{\mathrm{r}}^{\mathrm{opt}}$ for the given (r_1, r_2);

3. at last OCA2@CSL uses the parameters optimized so far to run again the `OCA2K` to test the porcessing error and the effective C_r on the same data in input or on another independent data chunck.

We recall that the X in Γ_X denotes the way in which the parameters are optimized, either trying to minize the processing errors on the differentiated data ($\Gamma_{\rm diff}$), on total power data ($\Gamma_{\rm sky}$) or on both ($\Gamma_{\rm sky,diff}$)

4 Validation of the OCA2@CSL analytical model with flight data

The critical point of a departure of the real signal from the hypothesis outlined in Sect. 3.1 is that the function of merith $\Gamma_X(r_1, r_2)$ used to indentify the best (r_1, r_2) combination is sensitive to the statistical distribution of quantized data [AD-1]. Indeed, γ_q has the form

$$\gamma_q(r_1, r_2) \propto \frac{q_{\rm opt}(r_1, r_2)}{\epsilon_{q=1}(r_1, r_2)}; \tag{1}$$

where $\epsilon_{q=1}(r_1, r_2)$ is an analytical function expressing the processing error as a function of (r_1, r_2) for quantization step $q = 1$, while $q_{\rm opt}(r_1, r_2)$ is the quantization step which has to be applied to the mixed data in order to reach the required compression rate $C_{\rm r}^{\rm opt}$. Best (r_1, r_2) are those for which $\gamma_q(r_1, r_2)$ has an absolute maximum.

While for $\epsilon_{q=1}(r_1, r_2)$ an analytical formula exists, there is no way to derive any general formula for $q_{\rm opt}(r_1, r_2)$ [AD-1]. As a consequence either $q_{\rm opt}(r_1, r_2)$ is either derived numerically by using the slow onboard processing emulator, or by using an analytical approximation described in [AD-1] and based on the hypothesys in Sect. 3.1.

The effect of the departure on these hypothesys has to be evaluated on a case–by–case basis on real data.

4.1 Data used for the validation

To validate the analytical model of OCA2@CSL with flight data we used chuncks of nominal AVR1 data acquired for the REBA calibration during OD–62 [RD-1], when chunks of 45 minutes of AVR1 data have been acquired with nominal $N_{\rm aver}$ for each detector. Not to violate the telemetry constraints, detectors have been acquired in nominal AVR1 according to a rotation scheme.

Since `OCA2K` is more than one order of magnitude slower then `OCA2K` the test have been caried on chunks of 5 minutes of data which have been selected to be statistically representative of the 45 min chuncks.

4.2 Validation algorith

The validation procedure is based on the following scheme:

1. a grid of 26×26 combinations of (r_1, r_2) with $-2.5 \leq r_1, r_2 \leq +2.5$ has been defined and resolution $\delta r_1 = \delta r_2 = 0.2$;

2. for each detector `OCA2K` have been used to scan the grid by computing the compression rate for two values of quantization step: q_1 and q_2 giving respectivelly $C_{{\rm r},1}$, $C_{{\rm r},2}$;

3. as a default $q_1 = 1$, $q_2 = 0.5$; but if for a given combination of (r_1, r_2, q) REBA saturation occurs [AD-1] then the range of q have been varied to have $q_1 = q_{\rm min}$, and $q_2 = q_{\rm min}/2$ where $q_{\rm min}$ is the smallest q for which REBA saturation is avoided;

4. by using

$$\log q_{\rm opt} = \frac{\log q_2 - \log q_1}{\frac{1}{C_{{\rm r},2}} - \frac{1}{C_{{\rm r},1}}} \left(\frac{1}{C_{\rm r}^{\rm opt}} - \frac{1}{C_{{\rm r},1}} \right) + \log q_1, \tag{2}$$

the $q_{\rm opt}$ for the given $C_{\rm r}^{\rm opt} = 2.4$ have been derived;

5. from the r_1,.r_2 and the numerical $q_{\rm opt}$ the total power quantization errors: $\epsilon_{q,\rm sky}$, $\epsilon_{q,\rm ref}$, and the quantization error for differentiade data $\epsilon_{q,\rm diff}$ have been derived, and from that the tabulated functions of merith for optimizzation of differentiated data, $\Gamma_{\rm diff}$, of total power data, $\Gamma_{\rm sky}$, and of optimization of differentiated and total power at once, $\Gamma_{\rm sky,diff}$, have been derived (see [AD-1] for exact definition of all of these quantities).

The same procedure have been applied by using OCA2@CSL and the corresponding functions of merith have been compared.

The time to test each of the 44 radiometers with `OCA2K` is about 12 minutes and the whole simulation takes nearly 9 hours. The same simulation with OCA2@CSL, takes half an hour.

4.3 Validation results

Fig. 2 and Fig. **??** compares the Γ_X from `OCA2K` and OCA2@CSL. Differences in the two distributions are evident, albeit not large. Basically the analytical approximation gives Γ_X functions a bit more peaked than the numerical solution. The REBA saturation does not affect the profile occurring very far from the peaks. The peaks, corresponding to the optimal r_1, r_2 parameters are shifted of an amount comparable to the grid resolution.

To measure the shift of the peak in a quantitative manner we define an optimal solution shift

$$\Delta_{\rm opt} = \sqrt{(r_1^{(\rm numerical)} - r_1^{(\rm analytical)})^2 + (r_2^{(\rm numerical)} - r_2^{(\rm analytical)})^2}, \tag{3}$$

Fig 3 gives the $\Delta_{\rm opt}$ for the $\Gamma_{\rm diff}$, $\Gamma_{\rm sky}$ and $\Gamma_{\rm sky,diff}$ of 44 LFI detectors. All the solutions are shifted of some amount, $\Delta_{\rm opt} = 0$ simply are shifted of an amount smaller than the grid resolution, 0.2, The worst shifted solutions are those for $\Gamma_{\rm sky,diff}$ of some of the 40 GHz detectors, for which $\Delta_{\rm opt} = 0.8$ but in general the shifts are not larger than 0.3. The worst shifts occurs for the $\Gamma_{\rm sky}$ and $\Gamma_{\rm sky,diff}$

To measure the variation of processing errors for optimizing Γ_X numerically or analytically we defined the ratio:

$$\mathcal{R}_X = \frac{\epsilon_{q,X}^{(\rm numerical)}}{\epsilon_{q,X}^{(\rm analytical)}}, \tag{4}$$

where $\epsilon_{q,X}^{(\rm method)}$ is the quantization error for the given optimization method and function of merith.

Fig 4 represents $\mathcal{R}_X$ as a function of the detector for "diff" (top), "sky" (middle) and "diff–sky" (bottom) optimization. In general things does not change too much from analytical to numerical optimization. In some cases a noticeable improvement is evident, in others on the contrary, the numerical solution is worst. However it has to be noted that given the coarse resolution of the r_1, r_2 grid the selected solutions with both the analytical and numerical method are sub–optimal. A deeper investigation of this point is out of the scope of this simulation, but see Sect. 5.

4.4 Conclusions on validation

Numerical approximations are quite good in CSL as well as in flight in performing a first order optimazion of the REBA parameters.

However in flight the analytical approximation has to be completed by a more refined numerical step exploring the neightbours of the analytical best solutions. See. 5 for more details on this subject.

5 Hiper fine optimization

The arugments presented in Sect. 4, as well as the experience with `OCA2K` at RAA tests, CSL tests and some flight data, shown that rarelly after optimization the exact $C_{\rm r}^{\rm opt}$ is reached, typically some differences at the level of several percents are present. What is wors, the total bit rate is usually a bit higher than expected from the averaged compression rate.

A number of second order effects concurs in producing this missmatch:

1. finite resolution of r_1, r_2, and $q_{\rm opt}$ search grids;
2. non idealities in the signals (sky and ref are not white noises);
3. packets have finite size, leading to unefficient compression due to the compressor learning curve;
4. Total bit rate is dominated at second order by packets with low compression rate;

5.1 Hiper fine optimization method

The method is a trade–off between a full numerical optimization and a full analytical optimization. It is based on a hierarchical exploration with `OCA2K` of a region arount the optimal parameters analytically determined with a quite fine step in r_1, r_2 and in quantization step.

For each of the $GMFO$, $GMFT$ combinations a polynomial is fitted on $1/C_{\rm r}$ against $\log q$.

Also a polynomial is fitted for ϵ_q/q [1] as a function of r_1, r_2. The r_1, r_2 leading at a minimum ϵ_q/q is taken.

After that the optimal $\log q$. is derived from the polynomial expansion of $1/C_{\rm r}$ against $\log q$.

5.2 Hiper fine optimization method

Fig 5 shows an example of such procedure applied at CSL data.

The plot shows the processing error for sky and ref as a function of compression rate before and after the hiper fine optimization is applied to standard OCA2@CSL optimization.

Before this optimization step we have had average compression rate $C_{\rm r} = 2.35 \pm 0.03$ (1σ). After it $C_{\rm r} = 2.39 \pm 0.01$ (1σ).

The processing error on differentiated data does not improve than of some percents, but the processing error on differentiated data improves of about 30%.

The *Hiper Fine Optimization* procedure is performed at the end of the OCA2@CSL processing, (it does not modify OCA2@CSL) to improve the accuracy in the solution search.

The time needed for optimization increased of about 6 – 10 minutes for each detector. The total time for optimazion with this step is about 7 – 8 hours.

[1] At first order $\epsilon_q \propto q$.

6 The real sky: Dipole and Galaxy

At odd with the hypothesys in Sect. **??** the real sky signal has deterministic comoponents which can not be approximated as normal distributed noise. The most importants are the Cosmological Dipole and the Galaxy.

The main concerns for the Dipole are that

1. it flattens the distribution of sky samples;
2. it increases the variance of the sky;

both of them changes the entropy of the signal potentially reducing the compression rate [RD-3] or forcing to increase q and then the processing error.

In addition the Galaxy is expected to make asymmetric the distribution of sky samples, but since it affects less samples per packet than the dipole, it is not expected to be a major concenr [RD-3].

A side effect of the dipole and other real sky signals is that they make difficult to estimate the level of noise in the signal. Simple methods to remove the dipole and Galaxy component when estimating the noise has to be included in the flight model of `OCA`.

6.1 Simulating the dipole

The effect of dipole have been simulated by adding at a real data stream from CSL tests a sinuosoidal component of given amplitude and period sampled at the same times.

To avoid to consider the absolute calibration, the dipole amplitude $\mathcal{A}$ is espressed in units of the rms of noise for differentiated data, $\sigma_{\rm noise,diff}$, for the given detector. We take $\mathcal{A} = 0$, 1, 2, 3 and 4 times $\sigma_{\rm noise,diff}$. This covers all the possible ranges of dipole amplitudes since it is expected $\mathcal{A} \leq 3 \times \sigma_{\rm noise,diff}$ for all the detectors.

We considered a dipole period of 60 sec and we compare the outcome of Hiper fine optimization with that of the standard OCA2@CSL optimization.

6.2 Results

Of course the dipole does not affect the attainable $C_{\rm r}$, given `OCA2` optimizes the $C_{\rm r}$, but of course the dipole affects the processing error.

Fig. 7 shows the relative increase of the processing error as a function of $\mathcal{A}$ for each of the detectors of Feed Horns 18 and 26. The top plot, for each detector, it is shown $\epsilon_{q,\rm diff}(\mathcal{A})/\epsilon_{q,\rm diff}(\mathcal{A} = 0)$ for standard OCA2@CSL optimization (black) and Hiper fine optimization (red). In the bottom plot, for each detector, it is shown $\epsilon_{q,\rm sky}(\mathcal{A})/\epsilon_{q,\rm sky}(\mathcal{A} = 0)$ (black) and $\epsilon_{q,\rm ref}(\mathcal{A})/\epsilon_{q,\rm ref}(\mathcal{A} = 0)$ (red) for Hiper fine optimization. Here the standard OCA2@CSL optimization is not shown since it gives much worst results.

The main conclusion which may be drawn from these plots are:

1. The Hiperfine optimization is a up to a 50% better than the standard optimization.
2. Assuming Hiper fine optimization we see up to a 45% increment of $\epsilon_{q,\rm diff}$ due to dipole, and a more worst result occurs in total power;
3. There are big differences among FHs, likely due to the relative amount of white noise with respect to the 1/f noise, this could be at the root of the differences among detectors of feed horn 26 and 18

4. the behaviour is not just when the dipole becomes very strong, this is an unrealistica case, as noted before;

6.3 Conclusions

Dipole affects in a significant manner the optimization performances of at least some of the detectors. It is likely that in flight there will be the need to monitor the optimization against the mothly dipole variations.

7 R factor determination

The CSL tests where aimed at optimizing the compression while reducing as more as possible the processing error on differentiated data. This results in quite large processing errors in total power, i.e. for sky and ref taken singularly. There are a number of potential applications which could affected by an increase in the processing error in total power. A good application representative of them is the r determination based on compressed data. The required relative accuracy for such determination shall not be worst then 10^{-4} and with target 10^{-5} [AD-2].

7.1 Analysis

The r could be determined either as [AD-2]

$$r = \frac{\overline{T}_{\rm sky}}{\overline{T}_{\rm ref}}, \tag{5}$$

where $\overline{T}_{\rm sky} = {\rm mean}(T_{\rm sky})$, $\overline{T}_{\rm ref} = {\rm mean}(T_{\rm ref})$; or as

$$r = \frac{{\rm var}(T_{\rm sky})}{{\rm var}(T_{\rm ref})}, \tag{6}$$

both methods are sensitive to quantizzation but in a different manner. However the second method is not suitable for automated execution in the pipeline and then it is not considered in this analysis.

Error propagation could be applied at Eq. 5 to derive a general formula for the accuracy of the r determination,

$$\left(\frac{\delta r}{r}\right)^2 = \frac{1}{n_{\rm samples}}\left[\frac{\sigma^2_{\rm sky}}{\overline{T}_{\rm sky}} - 2\frac{\sigma_{\rm sky,ref}}{\overline{T}_{\rm sky}\overline{T}_{\rm ref}} + \frac{\sigma^2_{\rm ref}}{\overline{T}_{\rm ref}}\right], \tag{7}$$

where $\sigma_{\rm sky}$, $\sigma_{\rm ref}$ and $\sigma_{\rm sky,ref}$ are the elements of the matrix of covariance of the errors on sky and ref, and $n_{\rm samples}$ the number of $T_{\rm sky}$, $T_{\rm ref}$ couples considered.

For the quantization error, from [AD-1], Eq. (7) translates into

$$\left(\frac{\delta_q r}{r}\right)^2 = \frac{q^2}{12}\frac{1}{(r_2 - r_1)^2}\left[\frac{r_1^2 + r_2^2}{r^2} - 2\frac{r_1 + r_2}{r} + 2\right]\frac{1}{\overline{T}_{\rm ref}}\frac{1}{n_{\rm samples}}, \tag{8}$$

where we have considered than $\overline{T}_{\rm sky} = r\overline{T}_{\rm ref}$, this expression has a minimum whenever $r_1 = r$ or $r_2 = r$ for which

$$\left(\frac{\delta_q r}{r}\right)^2 = \frac{q^2}{12}\frac{1}{(r_2 - r_1)^2}\frac{1}{\overline{T}_{\rm ref}}\frac{1}{n_{\rm samples}}. \tag{9}$$

Eq. (8) depends on $1/\overline{T}_{\rm ref}$ and $1/n_{\rm samples}$, which is bad for optimizzation.

On the other side the limit on r determination is given by the instrumental noise. So instead of to put an upper limit for $\delta_q r$ due to quantization it is better to put a limit to the total δr or better on the ratio $\delta_q r/\delta_{\rm noise} r$ which does not depend on $1/\overline{T}_{\rm ref}$ and $1/n_{\rm samples}$.

$$\frac{\delta_q r}{\delta_{\rm noise} r} = \frac{q^2}{12}\frac{1}{(r_2 - r_1)^2}\sqrt{\frac{\frac{r_1^2+r_2^2}{r^2} - 2\frac{r_1+r_2}{r} + 2}{\frac{\sigma^2_{\rm sky}}{r^2} - 2\frac{\sigma_{\rm sky,ref}}{r} + \sigma^2_{\rm ref}}} \tag{10}$$

To put an upper limit on this ratio puts an exclusion in the r_1, r_2 space in a region sorrounding the line $r_1 = r_2$, at the opposite of the $\mathcal{Q}_{\rm ack}$ factor which excludes regions far from that line.

So combining those two exclusion we have a better delimitation of the region where to search for optimal REBA parameters

8 Failure of the additive model for the quantization noise

The model of quantization noise as a sort of addittive white, not–gaussian, noise which is at the root, as an example, of Sect. 3, and [AD-1], fails when q is too large with respect to the RMS of the signal. In the CSL tests we have had relatively large quantization errors in total power, and so we have been critical in this respect. This faillure could lead, as an example at a faillure in Reverie.

8.1 Monte Carlo simulation

A quantitative theory can not be easily derived for the general case, but the effect could be easily studied with Monte Carlo methods.

In particular we are interested at determining at which level of relative processing error, ϵ_q/σ, we could have such problem-

The Monte Carlo simulation is based on the following scheme:

1. 1000 Monte Carlo realization of random combinations of reba parameters;
2. equal probability for any combination;
3. applied at CSL 2600 test;
4. 1 hour of data about 1.7^3 samples;
5. $\epsilon_{q,\mathrm{ref}}/\sigma_{\mathrm{noise,ref}}$ for ref have been measured and compared to the theoretical expectation from [AD-1].

The result is shown in Fig. 8, where it is evident how at $\epsilon_{q,\mathrm{ref}}/\sigma_{\mathrm{noise,ref}} \geq 2$ there is an evident deviation from the ideal line $(\epsilon_{q,\mathrm{ref}}/\sigma_{\mathrm{noise,ref}})^{\mathrm{theory}} = (\epsilon_{q,\mathrm{ref}}/\sigma_{\mathrm{noise,ref}})^{\mathrm{measured}}$.

In particular measured quantization errors, are systematically underestimated. The figure shows that in CSL we have been very near to the critical line.

8.2 Analysis

It is easy to understand what is the cause of the faillure, quantization of a quantity X truncates values according to

$$X_q = q\mathrm{round}\left[\frac{X - \mathrm{mean}(X)}{q}\right] + \mathrm{mean}(X). \tag{11}$$

this process does not change the mean of X (at least as long as $\mathrm{mean}(X) \gg q$) but affects its variance. The relative measured quantization error is defined as

$$\frac{\epsilon_q}{\sigma} = \frac{\mathrm{RMS}(X_q - X)}{\mathrm{RMS}(X)}, \tag{12}$$

in the limit $q \to +\infty$, $\mathrm{round}\left[\frac{X-\mathrm{mean}(X)}{q}\right] \to 0$ and $\mathrm{RMS}(X_q - X) \to \mathrm{RMS}(X)$ so that $\epsilon_q\sigma \to 1$.

In few words a direct measure of the processing error for large q values, as done in OCA2@CSL and Reverie may result in a false acceptable quantization error both in total power and differentiated data.

In CSL, for some detector we have been near the critical region over which the analysis in OCA2@CSL and in [AD-1] fails.

As a cosequence the results of [AD-1] *cannot be easily extrapolated* to larger quantization steps, as those required to increase the compression rate.

8.3 Quock Index

In analogy to the $\mathcal{Q}_{\rm ack}$ index to check for REBA saturation we defined a $\mathcal{Q}_{\rm ock}$ index as

$$\mathcal{Q}_{\rm ock} = q\ \mathrm{MIN}\left(\frac{\mathrm{RMS}(Q_1)}{\mathrm{RMS}(P_1)}, \frac{\mathrm{RMS}(Q_2)}{\mathrm{RMS}(P_2)}\right); \tag{13}$$

where P_i, $i = 1, 2$ are the mixed data before quantization and where Q_i are the mixed data after quantization [AD-1].

A schematic representation of how the $\mathcal{Q}_{\rm ock}$ index works is in Fig. 9. For $q < \mathrm{RMS}(Q_i)$ the noise is addittive, and $\mathcal{Q}_{\rm ock} > 1$ and $d\mathcal{Q}_{\rm ock}/dq > 0$. As For $q > \mathrm{RMS}(Q_i)$ the quantization noise added by the quantization step is no more able to compensate the loss in variance of the signal, then $d\mathcal{Q}_{\rm ock}/dq < 0$, untill, increasing q a critical point is reached where $\mathcal{Q}_{\rm ock} < 1$.

9 Measure of a Periodic Signal in Total Power

What is the impact of quantization of total power on the measure of a pure sinusoidal signal?

This is an important asset, since it could be important, as an example, to be albe to detect as an example the effect of 4K ref fluctuations in the $T_{\rm ref}$ signal.

This is another important constrain, different from the r determination, since in the r the correlation between sky and ref quantization errors reduces the final impact on the quantization noise.

This is not the case for this kind of application.

9.1 Monte Carlo simulation

At the level of accuracy required by this study we perform a simple Monte Carlo under the conditions:

1. there is just an armonic component plu noise;
2. the period of this component is known;
3. amplitude and phases have to be determined.

The simulation was based on the following scheme:

1. the noise was provieded by 1 hour of data of the sky and ref from a 2600 data stream acquired in nominal conditions during CSL;
2. a Monte Carlo have been executed to sample a parameters space defined by

   r_1, r_2, q

   Amplitude, A, period, P, and phase, ϕ, of the sinusoid
3. The amplitude is espressed in units of RMS for the ref signal
4. the montecarlo sampled the parameters space $(r_1, r_2, q, A, P, \phi)$ assuming all the combinations are equiprobable.
5. The parameters of the sinusoid where in the range:

$$\begin{aligned} 0.1\ \mathrm{RMS}(T_{\rm ref}) \leq\ & A & \leq 1\ \mathrm{RMS}(T_{\rm ref}) \\ 2\ \mathrm{min} \leq\ & P & \leq 15\ \mathrm{min} \\ 0^\circ \leq\ & \phi & \leq 360^\circ \end{aligned}$$

9.2 Results

Fig. 14 shows the effect of quantization on the power spectrum evaluated at the sinusoid period P. Red stars are the values of spectral power without quantization, while yellow stars denotes the spectral power for the same realization but with quantization. Data are plotted as a function of $\epsilon_{q,\rm ref}/\sigma_{\rm noise,ref}$. It is evident a change at the crossing point where $\epsilon_{q,\rm ref}/\sigma_{\rm noise,ref} \approx 1$ i.e. when quantization becomes relatively large.

Fig. 11 shows the correlation between the input power spectra at frequency $1/P$ (i.e. the power spectra calculated on the pure sinusoid) and the output power spectra after having added the noise

but without quantization (red $*$) and with quantization (yellow $*$ and $\diamond$) In the ideal case all the data should concentrate around the $x = y$ line. The effect of quantization is evident as larger dispersion of the samples processed with a large quantization (yellow $\diamond$) with respect to the case of small quantization (yellow $*$) the latter being practically not distinguishible from the unquantized case. The effect of large quamtization is to increase of up to a factor of 10 the dispersion.

A better representation of the effect is in Fig. 12 which shows the ratios of power spectra with and without quantization. Again there is an evident difference between the low quantization and the hight quantization population. Also the effect does not depend on the amplitude of the sinusoid, while Fig. 13 shows clearly that there is not any dependence on the phases of the data.

The same plot but as a function of the period P is shown in Fig. **??** where it is evidenced a sensitivity of large quantization errors with the period.

9.3 Conclusions

TBD

10 Final remarks

TBD

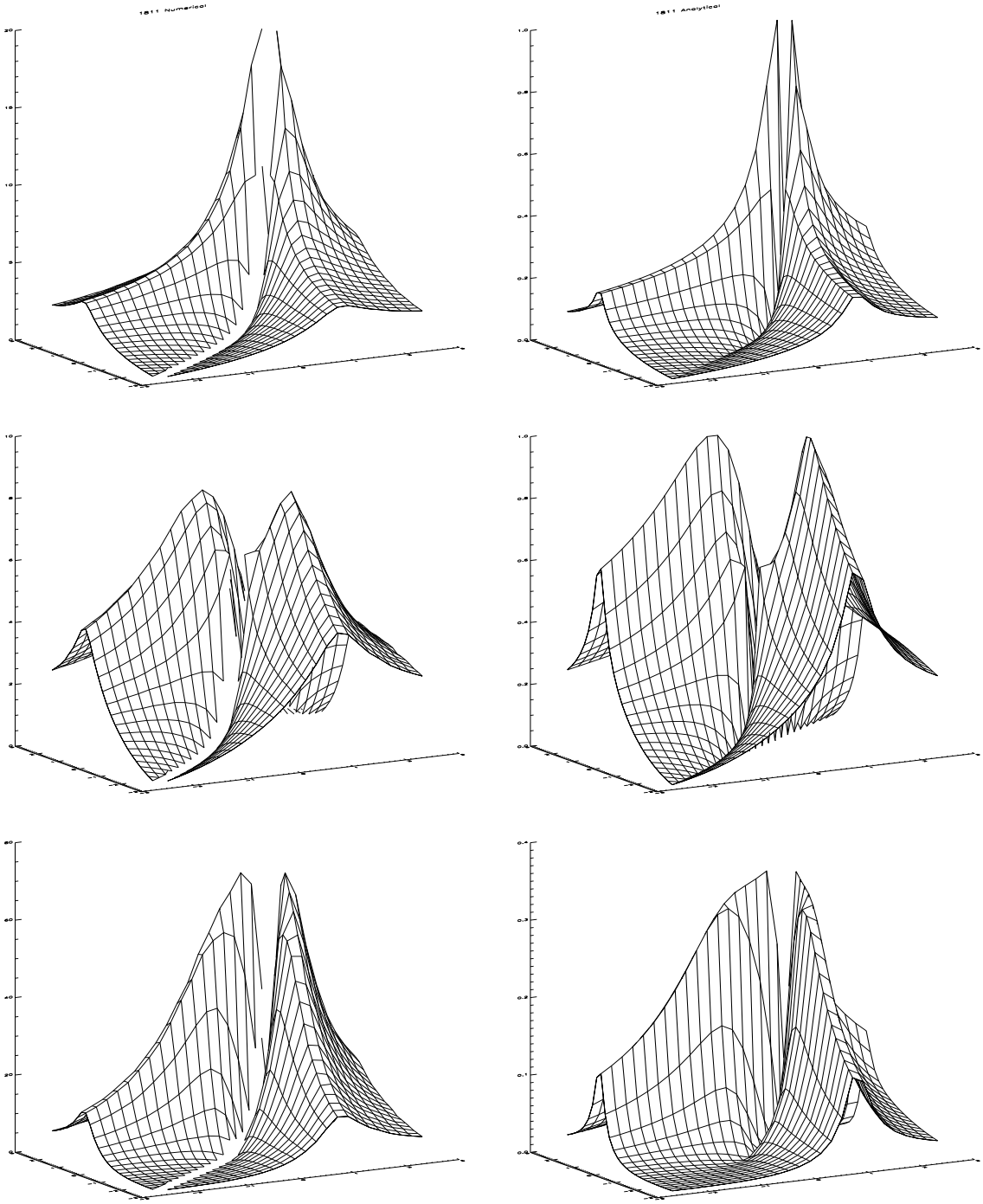

Figure 1: Comparison of Γ_X functions generated with a full numerical simulation (left) and an analytical optimization (right), for detector 1811. From top to bottom: $\Gamma_{\rm diff}$, $\Gamma_{\rm sky}$, $\Gamma_{\rm sky,diff}$.

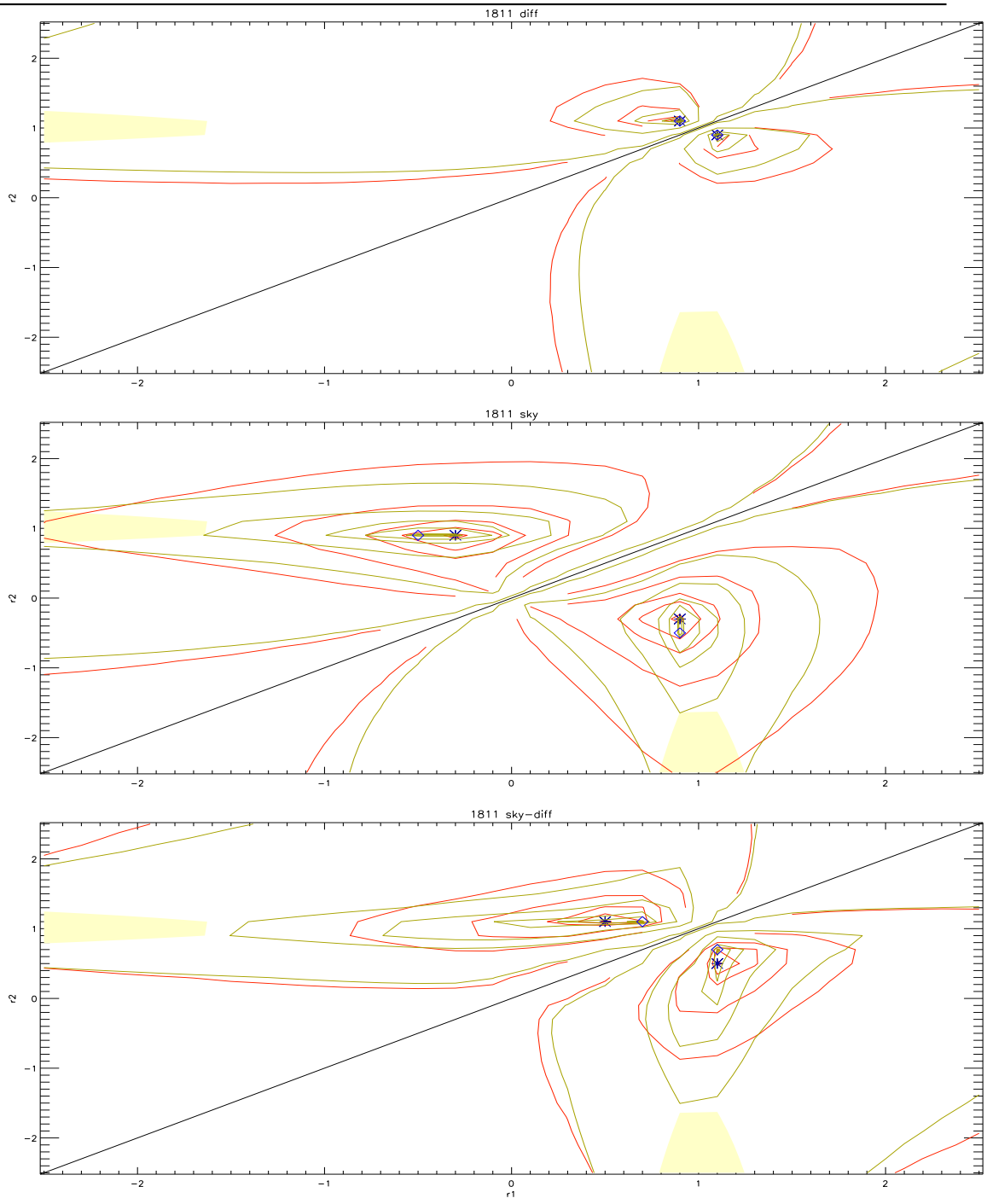

Figure 2: Comparison of Γ_X functions generated with a full numerical simulation (red lines) and an analytical optimization (green lines), for detector 1811. From top to bottom: $\Gamma_{\rm diff}$, $\Gamma_{\rm sky}$, $\Gamma_{\rm sky,diff}$. Yellow patches denotes (r_1, r_2) affected by saturation. Contour lines are for $\Gamma_X/\max(\Gamma_X) = 0.1$, 0.5, 0.75, 0.9, 0.95, 0.99, and 0.995. Stars ($*$) mark the best solutions for the numerical Γ_X function. Diaomond ($\diamond$) mark the best analytical solutions.

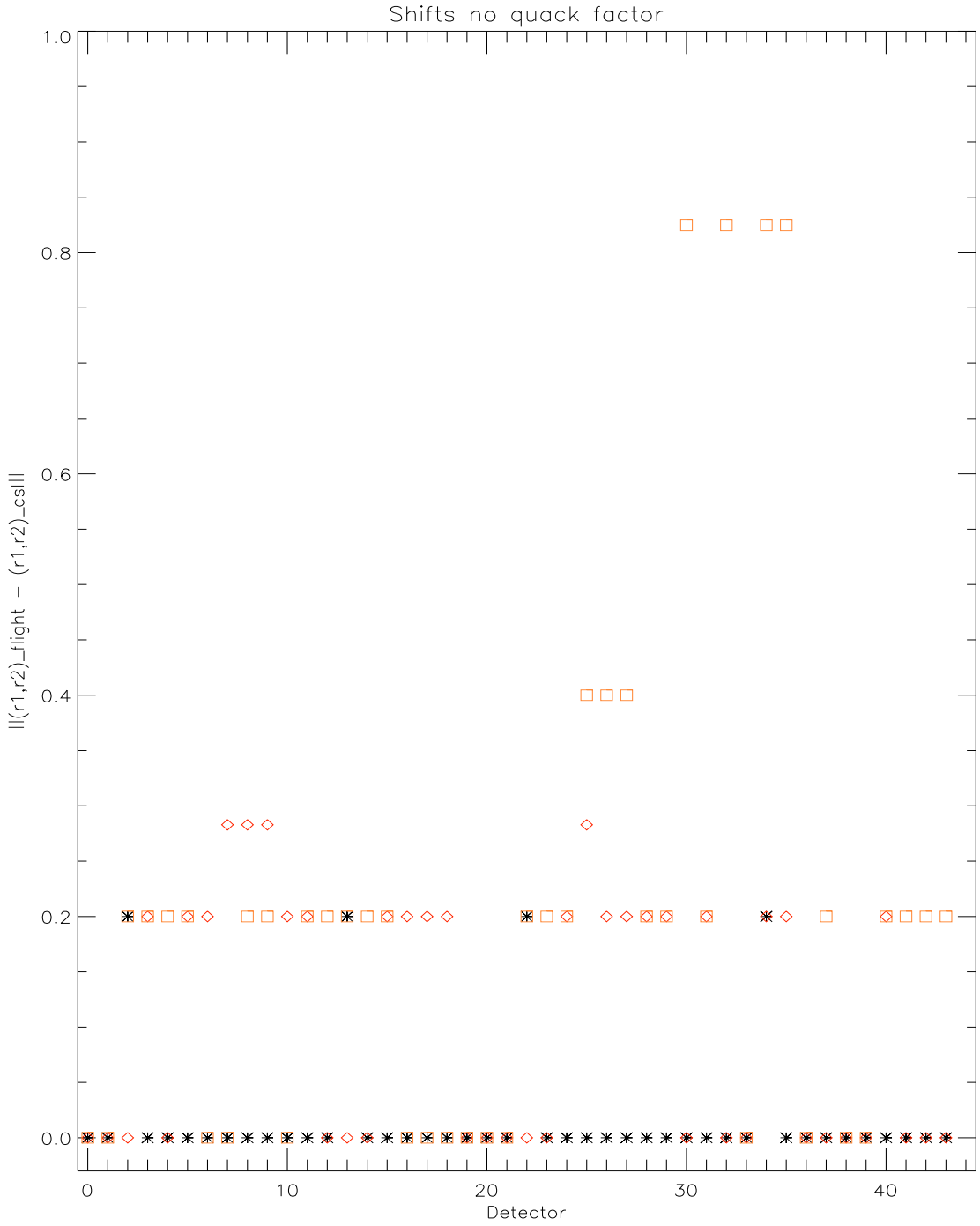

Figure 3: Values of $\Delta_{\rm opt}$ for the 44 LFI detectors. and $\Gamma_{\rm diff}$ ($*$), $\Gamma_{\rm sky}$ ($+$) and $\Gamma_{\rm sky,diff}$ ($\Box$). On the ordinate the detector index is ordered in the usual manner: 0 for 1800, 1 for 1801, ..., 43 for 2811. The step of the r_1, r_2 is 0.2 which fixes the minimum detectable shift.

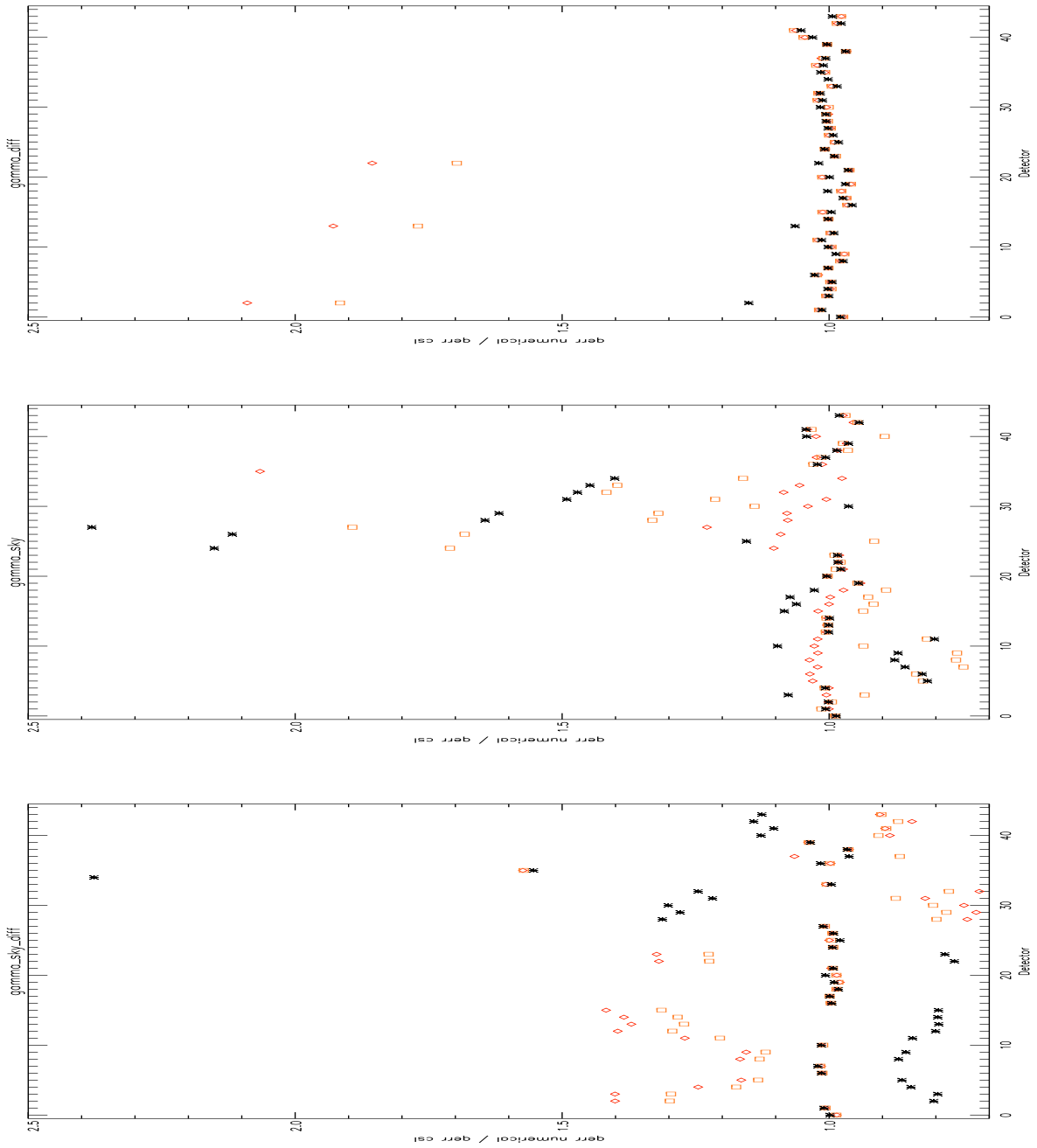

Figure 4: Values of $\mathcal{R}_X$ for the "diff" (top), "sky" (middle) and "sky–diff" (bottom) optimizzation of the 44 LFI detectors. In the plot ratios for $\epsilon_{q,\mathrm{diff}}$ ($*$), $\epsilon_{q,\mathrm{sky}}$ ($+$) and $\epsilon_{q,\mathrm{ref}}$ ($\square$) are shown.

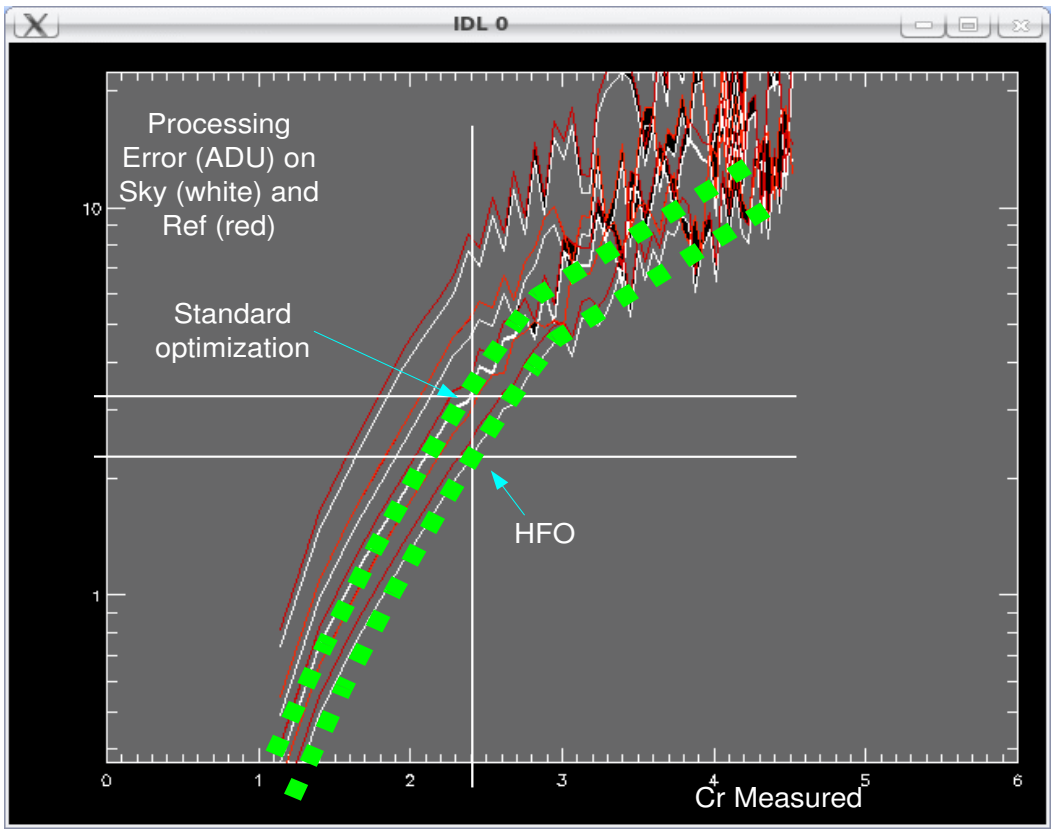

Figure 5: Example of Hiper fine optimization compared with standard optimization. The plot shows $\epsilon_{q,\mathrm{sky}}$ (white) and $\epsilon_{q,\mathrm{ref}}$ (red) as a function of measured C_r for a set of shifts about the optimal combination of r_1, r_2 parameters.

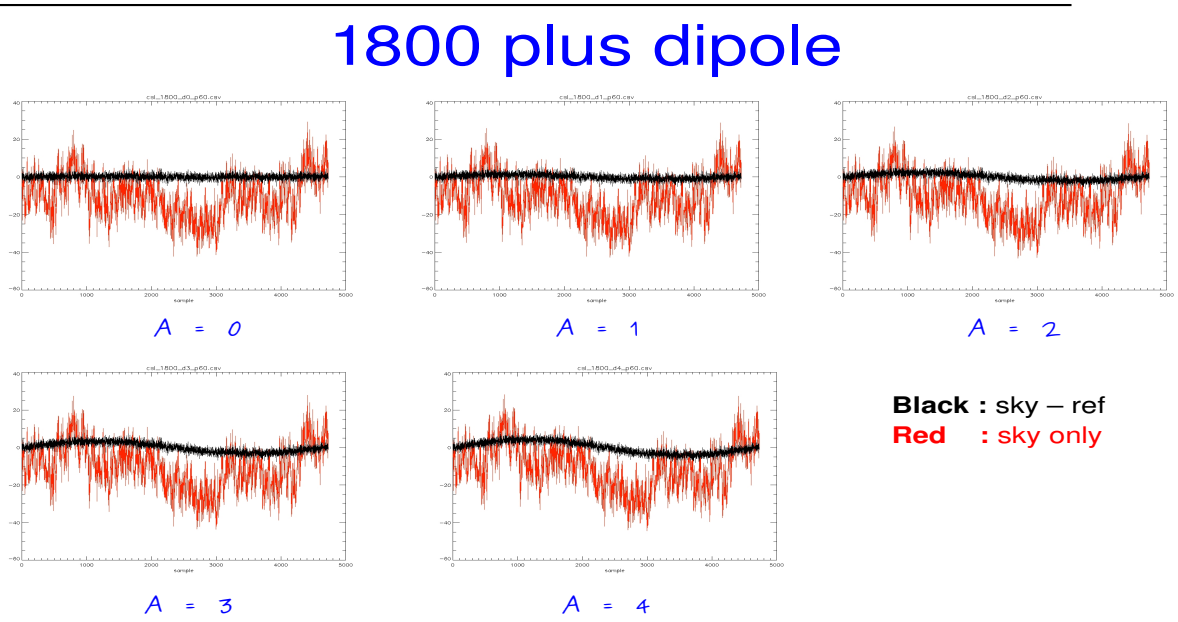

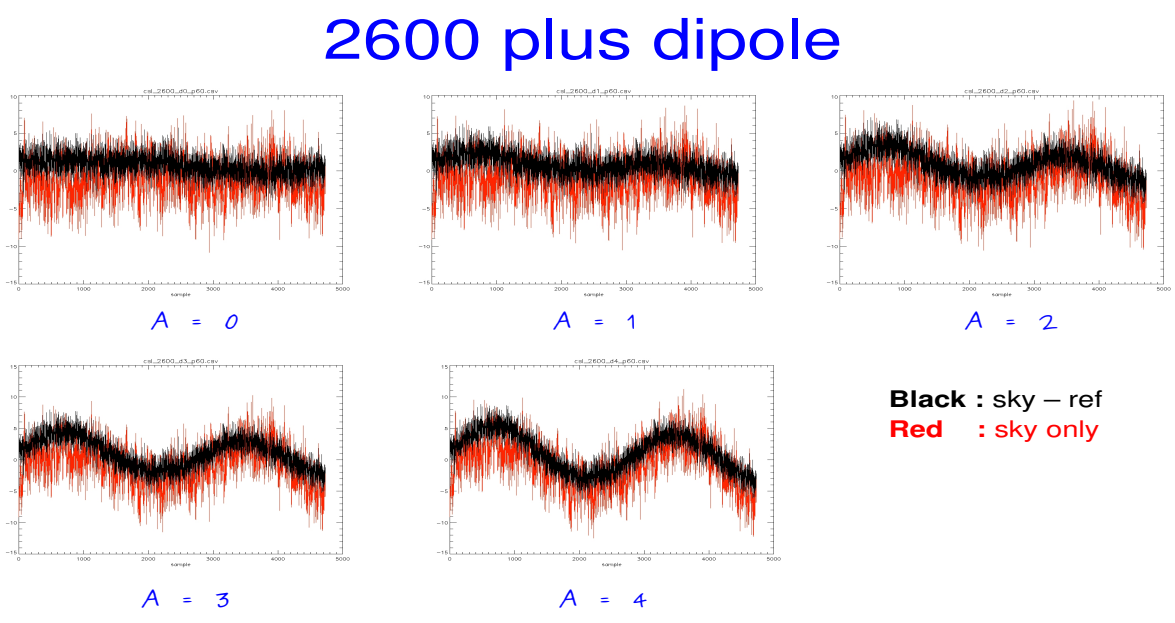

Figure 6: Example of simulated sky (red) and differentiated signals (red) from CSL with added dipole for detectors 1800 and 2600 as a function of relative dipole amplitude. For graphical purposes from the sky it have been removed the mean.

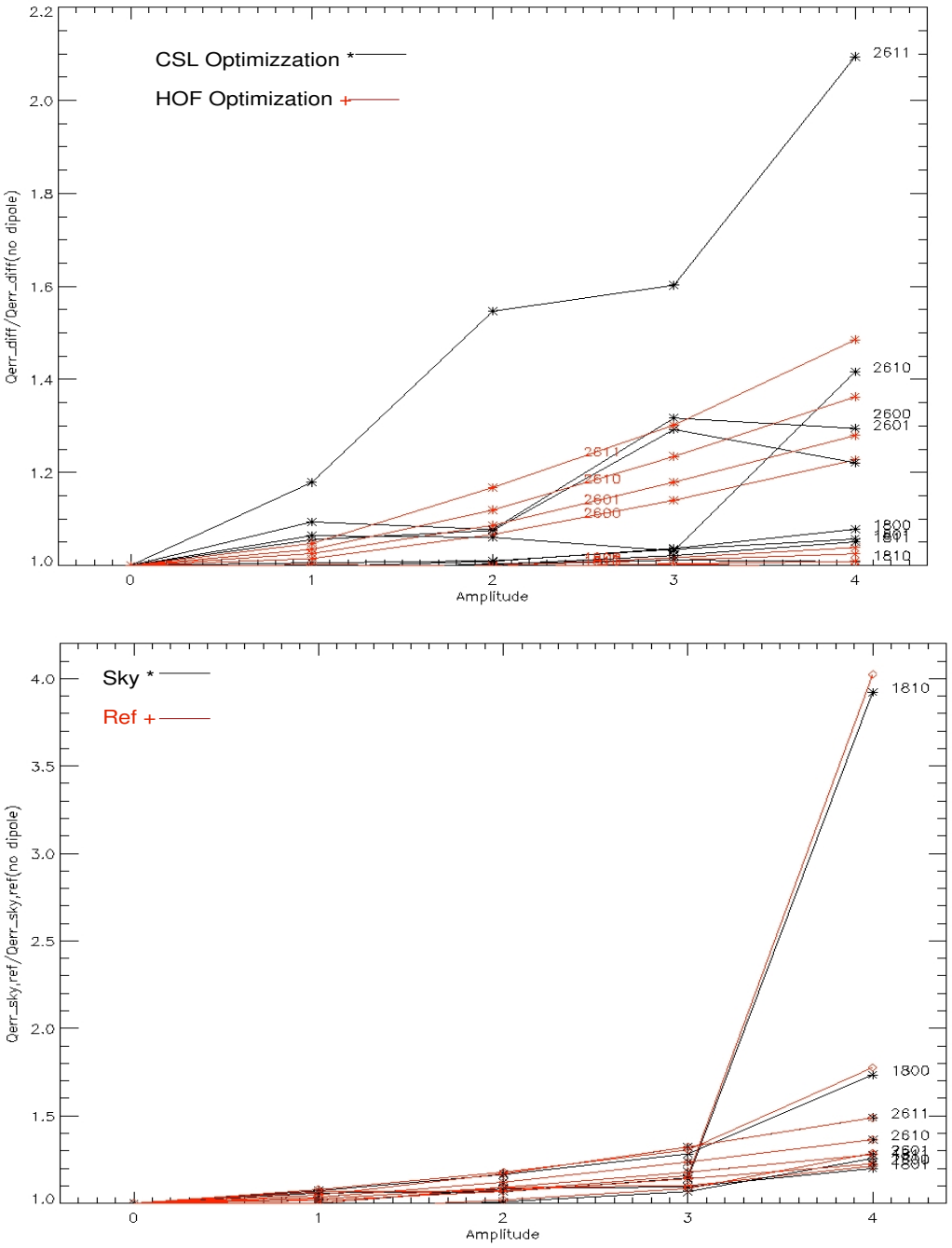

Figure 7: Increment of processing errors for differentiated data (top) and total power data (bottom) for compression optimizzed at $C_{\rm r}^{\rm opt} = 2.4$ adding the simulated dipole, as a function of the dipole amplitude in units of noise rms. Plots are for detectors of Feed Horns 18 and 26. In the top plot, for each detector, it is shown $\epsilon_{q,\rm diff}$ for standard OCA2@CSL optimization (black) and Hiper fine optimization (red) In the bottom plot it is shown $\epsilon_{q,\rm sky}$ (black) and $\epsilon_{q,\rm ref}$ (red) for Hiper fine optmization.

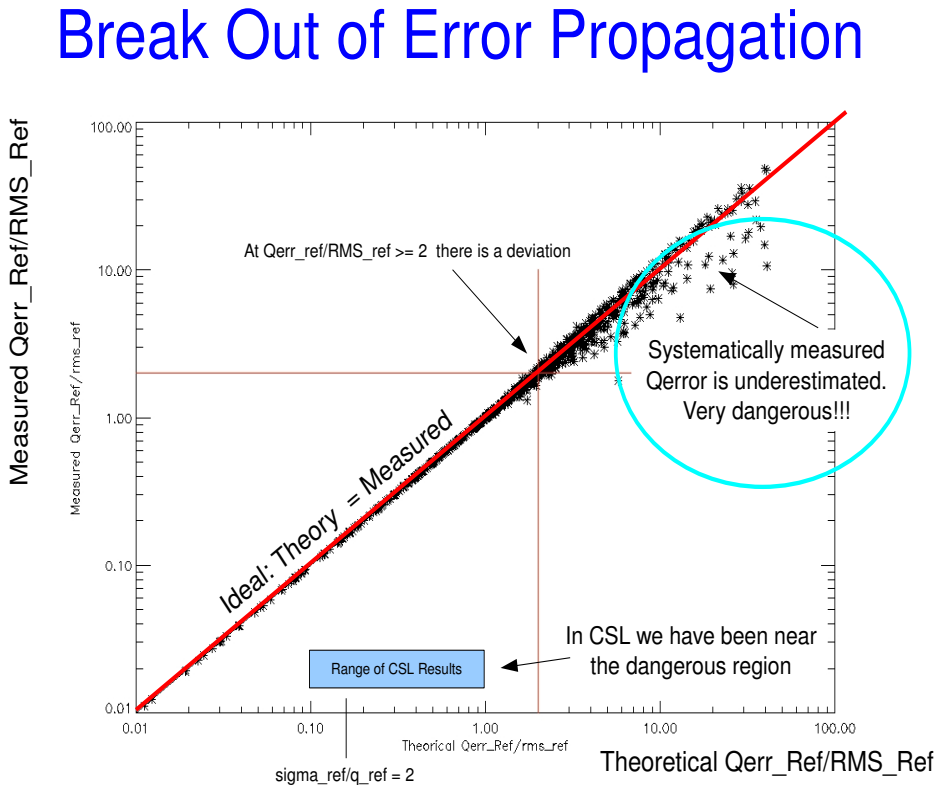

Figure 8: Monte Carlo analysis of processing error propagatioin faillure.

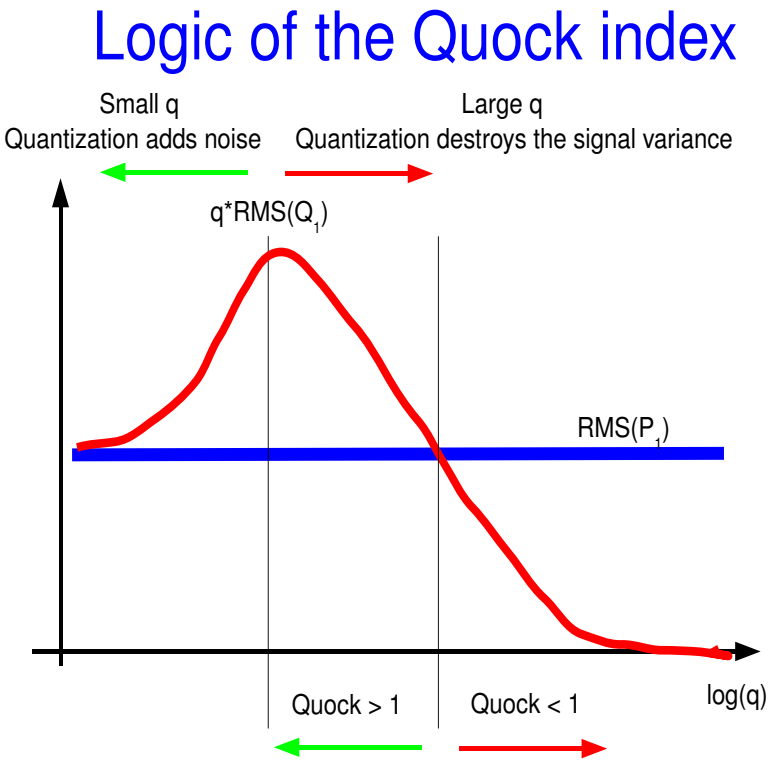

Figure 9: Schematic representation of the $\mathcal{Q}_{\rm ock}$ index.

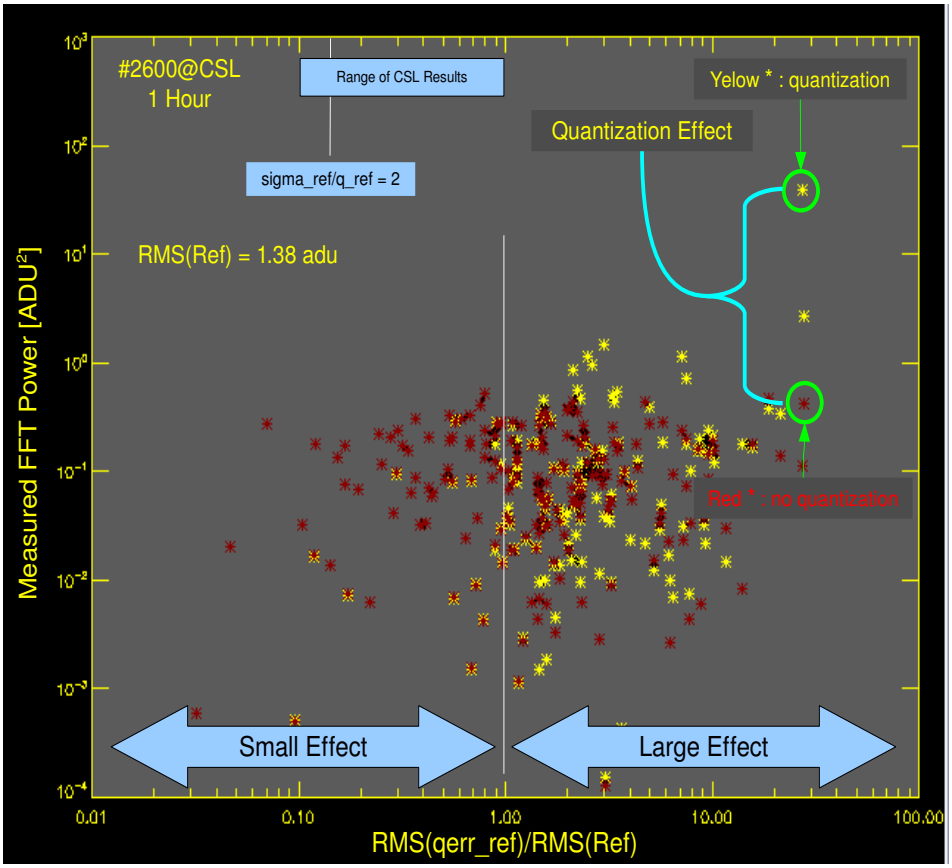

Figure 10: Effect of quantization on power spectra at the frequency $1/P$ and as a function of $\epsilon_{q,\mathrm{ref}}/\sigma_{\mathrm{noise,ref}}$. Red stars $(*)$ are the values of spectral power without quantization, yellow stars spectral power with quantization.

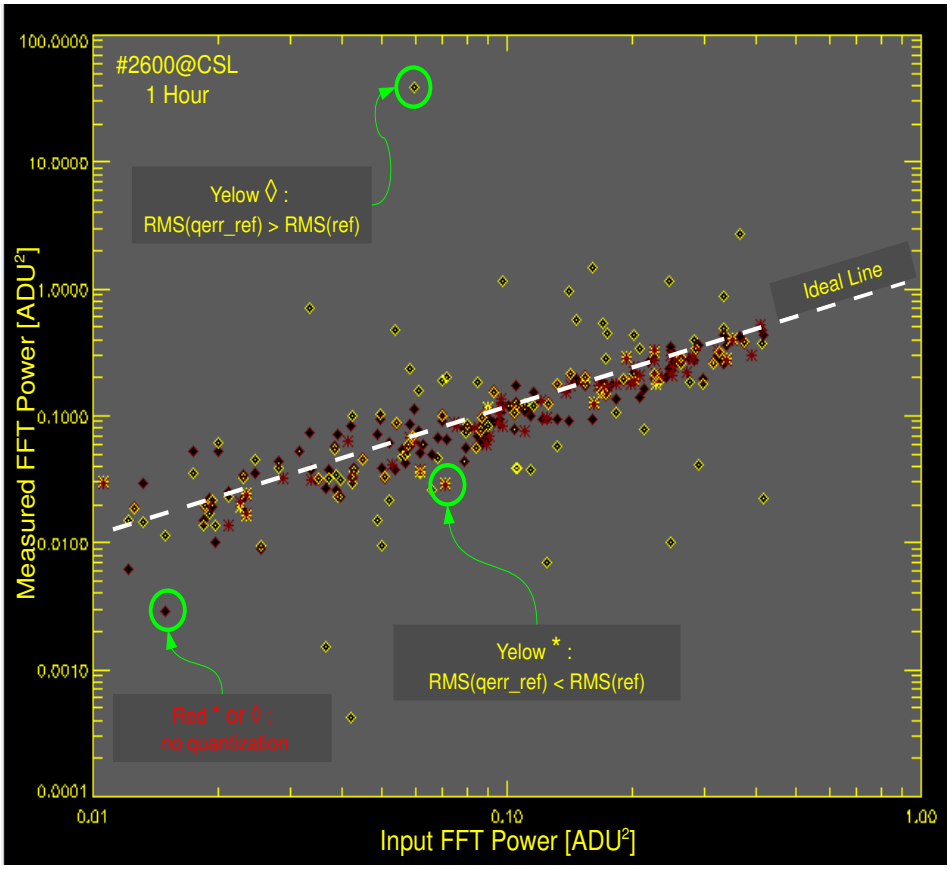

Figure 11: Comparison between the input power spectrum of the sinuoid and the output without quantization (red $*$) and with quantization (yellow $*$ and $\diamond$) at freqeuncy $1/P$. Here $(*)$ mark the samples with a small quantization, while $\diamond$ samples with a large quantization.

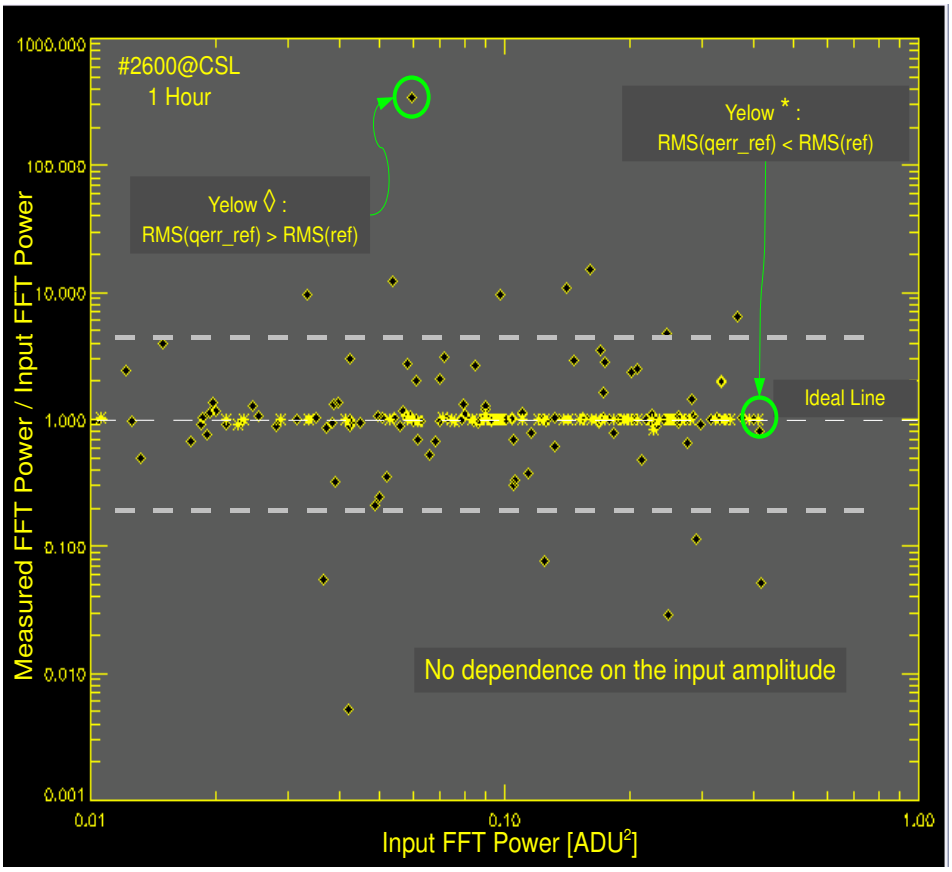

Figure 12: Ratios of power spectrum with quantization and of power spectrum without quantization at freqeuncy $1/P$, as a function of the power spectrum of the input sinusoid. Here $(*)$ mark the samples with a small quantization, while $\diamond$ samples with a large quantization.

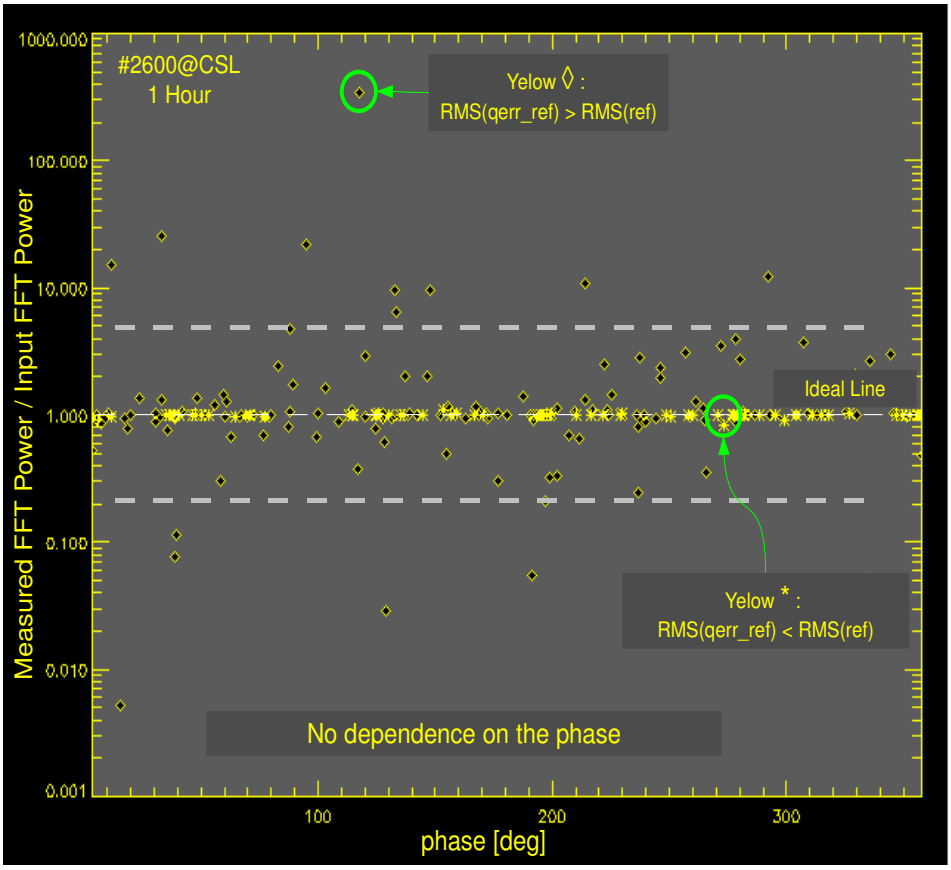

Figure 13: Ratios of power spectrum with quantization and of power spectrum without quantization at freqeuncy $1/P$, as a function of the phase of the input sinusoid. Here $(*)$ mark the samples with a small quantization, while $\diamond$ samples with a large quantization.

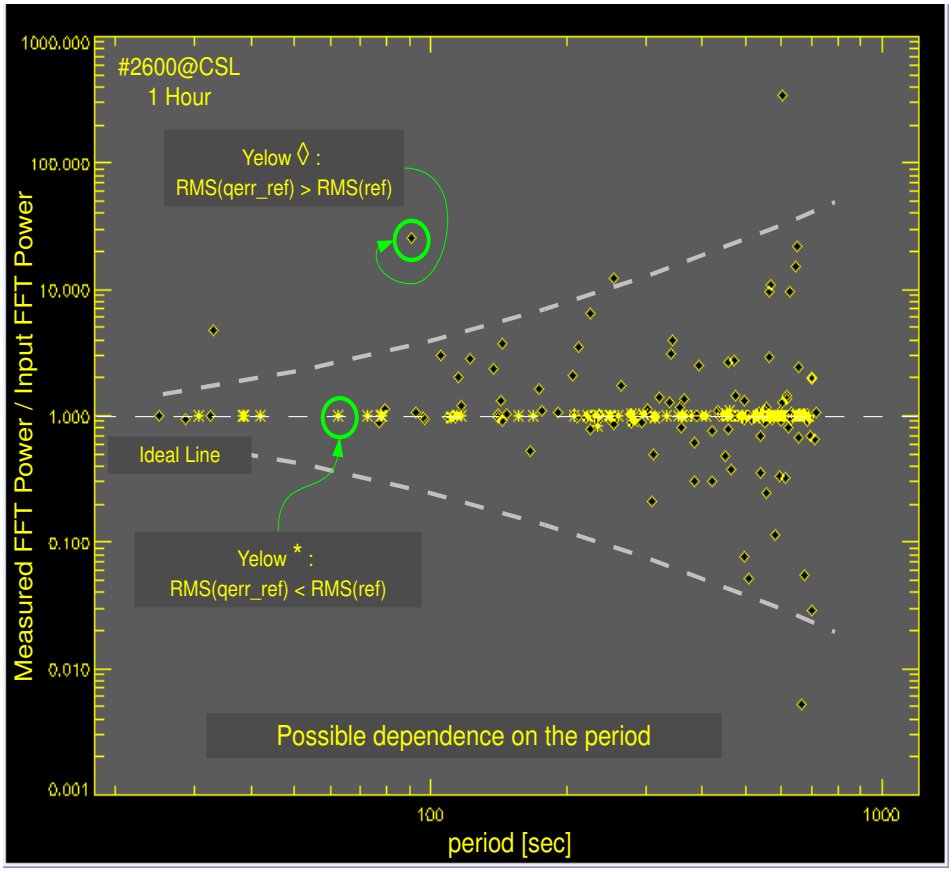

Figure 14: Ratios of power spectrum with quantization and of power spectrum without quantization at freqeuncy $1/P$, as a function of the period of the input sinusoid. Here $(*)$ mark the samples with a small quantization, while $\diamond$ samples with a large quantization.